CHALMERS

Modelling of the gas flow in fluidized beds

Master's Thesis - MSc programme in Innovative Sustainable Energy Engineering

FEDERICA GIOIA

Department of Energy and Environment
Division of Energy Technology
CHALMERS UNIVERSITY OF TECHNOLOGY
Göteborg, Sweden 2017

MASTER'S THESIS

Modelling of the gas flow in fluidized beds

Master's Thesis - MSc programme in Innovative Sustainable Energy

FEDERICA GIOIA

SUPERVISOR(S):

David Pallarès

EXAMINER

David Pallarès

Department of Energy and Environment *Division of Energy Technology*
CHALMERS UNIVERSITY OF TECHNOLOGY

Göteborg, Sweden 2017

Modelling of the gas flow in fluidized beds
Master's Thesis - MSc programme in Innovative Sustainable Energy
FEDERICA GIOIA

© FEDERICA GIOIA, 2017

Department of Energy and Environment
Division of Energy Technology
Chalmers University of Technology
SE-412 96 Göteborg
Sweden
Telephone: + 46 (0)31-772 1000

Chalmers Reproservice
Göteborg, Sweden 2017

Modelling of the gas flow in fluidized beds
Master's Thesis - MSc programme in Innovative Sustainable Energy
FEDERICA GIOIA
Department of Energy and Environment
Division of Energy Technology
Chalmers University of Technology

ABSTRACT

Fluidized bed technology plays an important role in the transition of the current energy system to full sustainability, both as main first choice for thermochemical biomass conversion (which is considered CO_2 neutral) and as basis for chemical looping combustion (CLC), which is considered to be the second generation of carbon capture applications, since it allows CO_2 capture with no inherent energy penalty.

The aim of the work is to formulate and implement a proper description of the gas flow inside a fluidized bed, covering a variety of scales and applications. This will be done by the development of an own code, since this provides enhanced flexibility with respect to already developed modelling tools available on the market. The influence of four parameters (inlet velocity, exchange coefficient between phases in the dense bed, dense bed height and lateral diffusion coefficient) in regular fluidized bed combustion is studied, in particular considering a lateral injection of volatiles resembling biomass combustion.

The results have been mostly in line with the expectations, showing a high dependence of the system from the gas mixing more than kinetics, and, on the other hand, that the exchange between phases in the dense bed and the dense bed height are not influential parameters.

Keywords: CCS, Emissions, Fluidized bed, Gas mixing, Multiphase flow

Contents

Acknowledgements

I would like to thank David Pallarès for the help and guidance in this work, and for his constant availability. Your support has been very important to me and it has allowed me to learn so much in these five months.

I would also to thank my family and the L4-group for their remote support and for the very productive exchange of ideas.

Finally I would like to dedicate a special thanks to Francesca Burgos, who has believed in me and pushed me to go along the path that led me here.

Federica Gioia, Göteborg, June 2017

Notations

Abbreviations

BFB	Bubbling Fluidized Bed
CaL	Calcium Looping
CFB	Circulating Fluidized Bed
CCS	Carbon Capture and Storage
CLC	Chemical Looping Combustion
FBC	Fluidized Bed Combustor

Roman upper case letters

A	Cell face area	$[m^2]$
A_{bed}	Cross sectional area of the dense bed	$[m^2]$
Ar	Archimedes number	[-]
C	Gas concentration	$[mol_i/mol_{tot}]$
CV	Cell control volume	$[m^3]$
D	Diffusion conductance at cell face	$[mol/s]$
D_{lat}	Lateral diffusion coefficient	$[m^2/s]$
F	Convective mass flux	$[mol/s]$
K_{eb}	Bubble-emulsion transfer coefficient	$[1/s]$
N_g	Total number of gas species	[-]
Pe	Peclet number	[-]
R	Universal gas constant	$[Pa\ m^3/\ Kmol\ ]$
Re	Reynolds number	[-]
S_Φ	General source term notation	$[mol/s]$
S_{exch}	Source term due phase exchange	$[mol/s]$
$S_{exp/contr}$	Source term due area expansion/contraction	$[mol/s]$
S_{gen}	Generated or consumed molar flow	$[mol/s]$
S_{hom}	Source term due to homogeneous reactions	$[mol/s]$
S_{in}	Inlet molar flow	$[mol/s]$
S_{out}	Outlet molar flow	$[mol/s]$
$S_{react,exch}$	Exchange source term due to non-equimolar reactions	$[mol/s]$
S_p	Slope of the linearized source term over the volume	[-]
S_u	Intercept of the linearized source term over the volume	$[mol/s]$
S_p^{BC}	Slope of the linearized source term over the volume due to the boundary condition set	[-]
S_u^{BC}	Intercept of the linearized source term over the volume due to the boundary condition set	$[mol/s]$
T	Operating temperature	[K]

Roman lower case letters

a	Discretized transport equation coefficient	$[mol/s]$
bub	Bubble phase	[-]
d_{bub}	Bubble diameter	$[m]$
em	Emulsion phase	[-]
err_{abs}	Absolute error	$[mol/s]$
err_{rel}	Relative error	[-]
$f_{i,r}$	Molar flow due to diffusion	$[mol/s]$
g	Gravitational acceleration	$[m/s^2]$
i	Gas species	[-]
j	Reaction number	[-]
mf	Minimum fluidization	
$\dot{n}$	Gas generation due to non-equimolar reactions	$[mol/s]$
nz	Node below dense/freeboard border	[-]
n_{nozzle}	Number of nozzles	[-]
$\vec{u}$	Gas velocity	$[m/s]$
u_g	Gas velocity from potential flow function	$[m/s]$
u_{mf}	Minimum fluidization velocity	$[m/s]$
u_s	Solids velocity from potential flow function	$[m/s]$
p	Operating pressure	$[Pa]$

Greek upper case letters

Γ	Diffusion coefficient	$[m^2/s]$
ϕ	General property notation	

Greek lower case letters

ε_s	Solids volume concentration	$[m^3/m^3]$
ρ	Partial gas density	$[mol/m^3]$
ρ_s	Averaged solids density in the given node point	$[kg/m^3]$

1 Introduction

Energy generation represents the main share of CO_2 production in Europe, and is thus a key field for countermeasures for the reduction of CO_2 emissions. Emission control in the energy field can be done in two main directions: renewable energy sources and current heat and power production control. The latter can involve either biomass conversion, exploiting the neutral CO_2 balance when applicable, through either combustion or gasification, or through the carbon capture technologies.

Carbon Capture and Storage (CCS) allows heat and power plants with non-renewable sources to reach a neutral balance in CO_2 emission. This technology is of particular interest to those countries that have high quantities of coal or oil available at a low price on the territory. Furthermore, often renewable energy cannot provide all the energy needed and is less economically feasible compared to existing plants from traditional energy sources. In fact, some of the renewable sources, such as solar or hydropower, are highly limited by the availability on the territory, so that it can be useful to limit the damages of traditional sources utilization for problematic zones.

It is also of particular interest the utilization of CCS with fuels that already have a neutral CO_2 balance, such as biomass. Biomass is not worldwide recognized as a sustainable energy source, since it depends on the forestal growth rate of each country. However, in countries where the sustainability characteristics are fulfilled[1], coupling biomass utilization and CCS (so-called BioCCS) results in a negative CO_2 balance, in which the net life cycle process results in a subtraction of CO_2 from the atmosphere.

Several studies [2] [3] foresee that additional CO_2 reduction measures will be needed in the future, which means that reducing the emissions could not be enough, but it would be necessary to remove the already released CO_2 from the atmosphere, and this can be achieved thanks to the synergy between forest growth, biomass utilization and carbon capture and storage technology.

The vast majority of the formerly described technologies for emission control involve the use of fluidised bed boilers, which will be the main focus of this work, and in some cases, as it will be explained in Section 1.3, fluidised beds represent the basis to the technology.

[1] The fulfilment could be defined, for example, with the fact that in spite of the biomass usage, the forestal growth rate is still positive at the end of the year in a considered Country. For example biomass is considered renewable in Sweden, which, although already considerably uses it for energy generation, presents so wide forestal area that the net growth rate is still positive at the end of each year [1].

1.1 Traditional CCS methods

CCS research started in 1970 and currently several technologies are, with many ongoing projects both in and outside Europe [4].

There are mainly three technologies for CO_2 capture: pre-combustion, post-combustion and oxy-fuel [5]. The first one involves the conversion of the fuel in hydrogen and carbon dioxide through gasification, so that CO_2 is removed from the resulting mixture before entering the combustion chamber. Post-combustion capture is based on the removal of CO_2 from the flue gases coming from a conventional plant through a sorbent, after having removed particulates and NO_x. Finally, oxy-fuel technology is quite similar to the pre-combustion, with the difference that nitrogen is separated from oxygen before entering the combustion chamber. Although technologies are available and, especially for the post-combustion, easy to integrate in existing power plants and industrial processes, their major issue is the energy penalty on the plant performances.

In fact, a consistent amount of heat is required for the capture process, which is usually extracted from the turbines, being the steam from the outlet of the turbine not enough for temperature requirement reasons. This obviously translates into a plant's efficiency drop, which depends on both the technology used and the capture efficiency, but that can reach 18% (roughly one fifth of the total energy) of energy penalty in an IGCC plant with more than 90% capture efficiency [6] [7].

Another CCS technology is the Calcium looping one. In CaL the flue gases from the combustor enter in a carbonator, where CO_2 reacts with CaO producing $CaCO_3$ at a mean temperature of 650℃. Then the $CaCO_3$ is recirculated in another reactor, called calciner, where the calcination of $CaCO_3$ is carried out at a higher temperature (~900℃) in a CO_2 rich environment. After this the sorbent is recirculated back to the carbonator, while the CO_2 exiting from the calciner is ready for compression and storage [8] [9].

1.2 Fluidized bed

Fluidized bed reactors offer several advantages with respect to traditional reactors. Taking combustion as example, the main idea is to feed and mix the fuel with a solids bed which has been fluidized with the primary gas injected from the bottom of the furnace, in order to improve the mixing between the fuel itself and the primary gas. In combustion, the injected gas can be either air or a mixture of air and recycled flue gas. Among other advantages there is surely the high efficiency and the inside temperature being fairly constant and quite low, normally around 850 ℃. This is beneficial for the NO_x production mechanism reduction, since this happens in presence of higher temperatures, but also because in these reactors the combustion is staged, which means that there is a secondary air injection. Furthermore, FBC units allow SO_2 capture by the addition of limestone in the bed. Fluidized bed are also very flexible in terms of

operation far from the nominal point and of fuel used, allowing gaseous, liquid and solid fuel in the reactor and absorbing fluctuations in fuel quality.

The combustor can be divided into two main areas: the dense bed, where most of the solid particles are located, and the riser, where the solids presence is limited. In between these two areas can be individuated a splash zone, which is a solid particles concentration transition area and where the solids follow ballistic movements. Depending on the superficial velocity of the injected air, the so called fluidization velocity, it is possible to divide the fluidized bed in two main categories: bubbling (BFB) and circulating (CFB) fluidized bed, whose schematics can be seen in Figure 1.

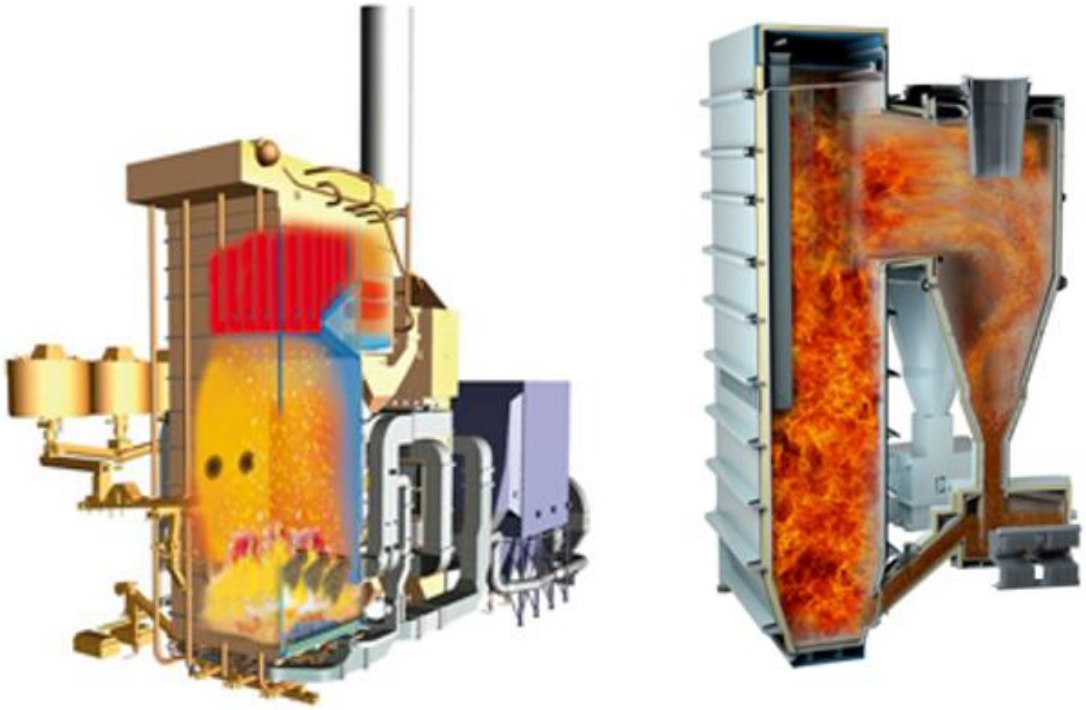

a) b)

***Figure 1**: a) BFB and b) CFB configuration. Retrieved from [10]*

The differences and principles of operation will be further discussed below. For both types of units, the bottom region is occupied by a dense bed in which there is formation of bubbles with low solids concentration in strongly oxidizing environment, while a second, dense phase (called emulsion) contains most of the solids (including solid fuel) and is in a reductive environment.

In bubbling fluidized beds (also called stationary fluidized beds) the primary gas velocity is kept very low but above the minimum fluidization velocity, which is the velocity that the particles have when the hydrodynamic drag force applied from the primary air equals the gravitational force of the particle. Still, the gas velocity is kept below the terminal velocity of the solids, so that no entrainment of particles from the bottom dense region to higher locations in the chamber occurs.

If the primary gas velocity is higher than the terminal velocity of a significant share of the particles, the FBC is called circulating, since there is a recirculation of the dense bed material. In particular, since the velocity is considerably higher than in BFB, the bed material, with decreasing size particle along the height of the reaction, will be in all the length of the combustor, which allows a more evenly distribution of the combustion in the FBC height with respect to BFB. The particles will afterwards enter in a cyclone that has the purpose of dragging the particles down to bottom of the furnace. The passage from the cyclone to the dense bed is done by effect of gravity. In the freeboard there is the formation of a main flow upwards, called core, and a lateral backward flow called layers, which contributes to part of the solids recirculation, and in which the gas velocity is to be considered approximately zero. CFB units require a higher capital investment and are thus typically not applied for thermal inputs below 50 MW.

1.3 Second generation CCS

Chemical Looping Combustion (CLC) is considered the technology for second CCS generation and is exclusively based on FB technology.

CLC (Fig.2) is realized by the use of a metal oxide which has the function of being the oxygen carrier, meaning that there is no direct contact between the combustion air and the fuel. CLC plants consist of two FB reactors, the air reactor, in which the oxygen carrier is oxidized with air (Eq. 1.1), and a fuel reactor, in which the oxidized metal oxide is reduced by the syngas (H_2 and CO, Eqs. 1.2 and 1.3) resulting from the gasified fuel, which therefore produces only H2O and CO_2, while the oxygen carrier is sent back to the air reactor to be oxidized again, closing the process loop.

The reactions taking place in the two reactors are Equation 1.1 for the oxidiser (called air reactor) and 1.2 and 1.3 for the reducer (called fuel reactor), respectively for combustion of hydrogen and carbon, while in Figure 2 is shown a scheme of CLC reactor working principle.

$$2\mathrm{Me} + O_2 \rightarrow 2MeO \quad (1.1)$$

$$2\mathrm{MeO} + H_2 \rightarrow 2Me + H_2O \quad (1.2)$$

$$MeO + CO \rightarrow Me + CO_2 \quad (1.3)$$

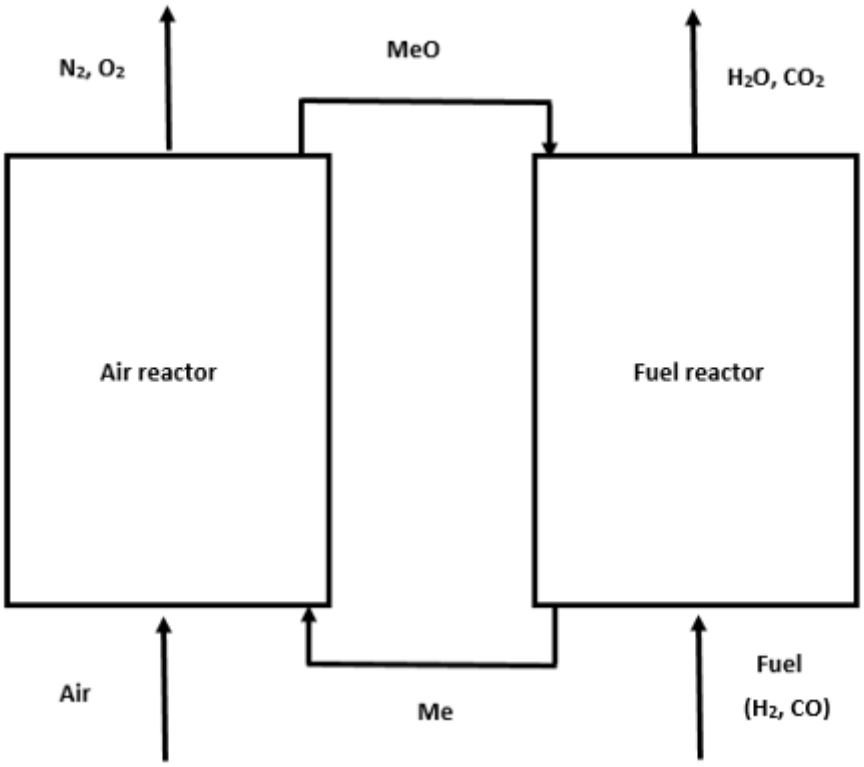

***Figure 2**: CLC reactor schematic*

In this way, the only gases present in the air reactor are N_2 and residual O_2, while in the fuel reactor only remain CO_2 and water vapour, which can be then easily expelled separately from the reactor [11] [12].

Thus it is the process itself that takes care of the CO_2 separation from the rest of the gases with no or very limited energy penalty on the overall efficiency. In fact, the only energy penalty would be constituted by the one needed for the CO_2 compression, which is, in any case, close to one fourth with respect to the penalty achieved with other CCS technologies [7].

1.4 Aim

The aim of this work is to produce a modelling tool for the gas flow in fluidized bed units. The model should be flexible in terms of being able to handle different applications. The model is used to investigate some sensitive factors in the air/fuel mixing and their influence on the process. In particular, the mass balances for six gaseous species will be solved in order to simulate their behavior and the parameters influence when considering lateral volatiles injection rather than a homogeneous air-volatiles mixture injection.

2 Theory

The modelling practice for reactors takes into account three transport equations: the momentum balances (from which the velocity fields are solved), the mass balances (from which concentrations are solved) and the heat balance (from which temperature is solved). While CFD calculations solve all of these, semi-empirical modelling solves only for mass and heat balances, while the momentum equation is not solved due to its computational cost. In the following sections will be given an overview of the theory behind the general form of the transport equation solved and how this is used in modelling, but also of the different modelling techniques, specifying which of the described have been used in this work and why, and finally of the structure of the developed code.

2.1 Transport equation

A transport equation is a differential equation expressing a certain conservation principle, be it in e.g. electromagnetic, fluid mechanics or thermodynamics. A transport equation can be described as the balance between diffusion, convection and, if existing, source terms. The transport equation for the general property Φ in its differential form can be written as follows [13]:

$$\frac{\partial(\rho\Phi)}{\partial \mathrm{t}} + \mathrm{div}(\rho\Phi\vec{u}) = \mathrm{div}(\Gamma grad\Phi) + S_\Phi \qquad (2.1)$$

Where the first term on the left represents the rate of increase of Φ, the second the net flow rate for Φ, the first term on the right is instead the net of increase of Φ due to diffusion and the second one is the rate of increase of Φ due to sources.

Being this study made with the finite volume method[2], (2.2) can be integrated in a three dimensional control volume, where is obtained:

$$\frac{\partial}{\partial \mathrm{t}}\left(\int_{CV} \rho\Phi \mathrm{dV}\right) + \int_A \hat{n}(\rho\Phi\vec{u})dA = \int_A \hat{n}(\Gamma \mathrm{grad}\Phi)dA + \int_{CV} S_\Phi\, dV \qquad (2.2)$$

In this way the first term on the left is the rate of increase of the property Φ in the control volume, the second term is the variation of Φ due to convection across the control volume boundaries, while the first term of the right is the variation of Φ due to diffusion and the second term is the creation of Φ inside the control volume.

[2] In the finite volume method the computational domain is divided in a finite amount of cells, each of which has a finite number of boundary faces. Those can be divided in internal and boundary faces, the former connecting two cells and the latter located at the border of the computational domain. The strength of FVM is that it only needs the flux evaluation for the cell boundary, which is applicable also to non-linear problems, and therefore make it interesting for non-linear conservation laws handling [14] [15].

In this work the flow will be considered at steady state, so that the first term on the left is set to zero. Therefore, eliminating the time-dependent contribution and integrating the previous between the boundary faces of the control volume cell it is obtained:

$$F\phi|_w^e + F\phi|_s^n + F\phi|_b^t = D\,\partial\phi|_w^e + D\,\partial\phi|_s^n + D\,\partial\phi|_b^t + \bar{S}\Delta V \qquad (2.3)$$

Where the convective conductance flow (F), the diffusion conductance at cell face (D) and the source term can in turn be defined as [9]:

$$F_i = \rho u A_i \qquad (2.4)$$

$$D_i = \frac{\Gamma_i A_i}{\partial r} \qquad (2.5)$$

$$\bar{S}\Delta V = S_u + S_p \Phi_p \qquad (2.6)$$

The transport equation can then be written in its discretized form, which is the form that will be used in the modelling through numeric methods.

In order to write the discretized transport equation for a steady state flow, it has firstly to be chosen the scheme of discretization. The discretization is the process that allows to continuous problems to be described in a discreet way, so that the notation is useful when using it during the modelling. In Figure 3 is shown the cell orientation convention used in this work:

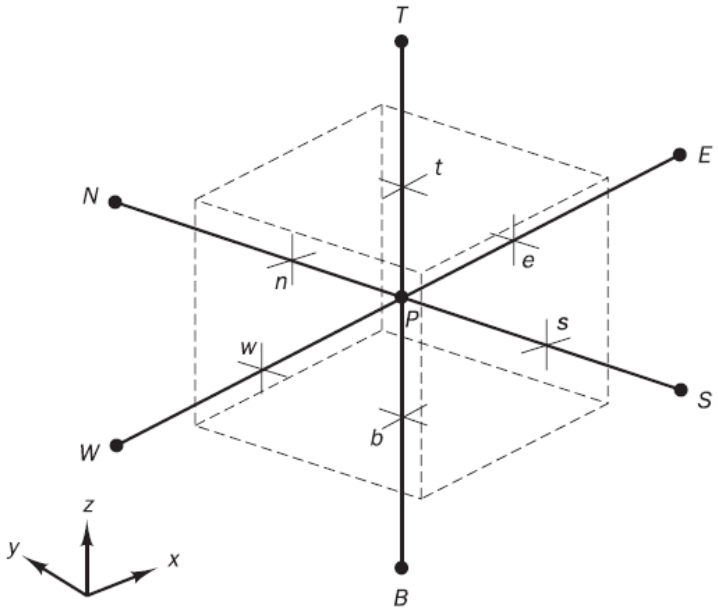

Figure 3: *Cell orientation rule. Retrieved from [13]*

In particular, in the finite volume method, the domain is divided in small control volumes, which have boundaries and a central node. In 3D the boundaries will be six in total, which are called north and south, east and west, and bottom and top.

During the discretization process the general property, which normally has a continuous form, is calculated in the node as a function of the property at the cell boundaries, where the function depends on the used scheme. The value at the cell boundaries is obtained from the values at the domain boundaries, usually specified in the boundary conditions.

Hereinafter follows a brief description of the principal schemes relevant for this kind of problems and their main characteristics.

2.1.1 Central differencing scheme

The central differencing scheme calculates the general property value in each node by doing a simple average between the values at the cell boundaries. Let us consider a 1D problem, as shown in Figure 4. If P is the considered node, let E and W be respectively the east and west neighbouring nodes, and *e* and *w* respectively the east and west cell boundaries.

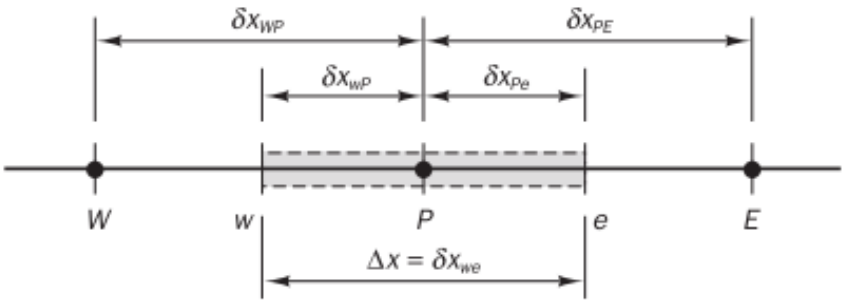

***Figure 4**: 1D representation of the cell and respective distances. Retrieved from [13]*

The property value at each cell boundary is calculated as an averaged value between the nodal points, i.e.:

$$\phi_w = \frac{\phi_P - \phi_W}{\partial x_{WP}} \tag{2.7}$$

$$\phi_e = \frac{\phi_E - \phi_P}{\partial x_{PE}} \tag{2.8}$$

The same is done with the other dimensions when considering a 3D problem. These mean values which are separately calculated for the three dimensions are then inserted in (2.3) to obtain the discretized equation.

The central differencing scheme satisfies the fundamental properties of conservativeness, boundedness and transportiveness which are necessary for the scheme's stability, however, by taking the average values for the property, this scheme does not take into account the direction of the flow, which is important especially when considering highly conductive flows.

2.1.2 Upwind scheme

In the upwind scheme the property evaluation takes into account the direction of the flow. In fact, while in the central differencing the calculation was only an average between the two nodal points, in the upwind the property value at a certain boundary face is taken as the value in the previous node, considering the direction of the flow. This means, referring to Figure 3, that if, for example, the flow goes from left to right,

the value in the west boundary face will be the value in the west point, while for the east face it will be the value in P.

The scheme respects the fundamental properties of conservativeness, boundedness and transportiveness, although giving some problems concerning false diffusion, meaning that it gives erroneous results when the flow is not in line with the mesh grid, with the error growing the coarser the mesh.

2.1.3 Hybrid differencing scheme

The hybrid differencing is a combination of the central differencing and the upwind schemes. In fact, it considers the first one for low Peclet numbers[3] and the second one when the Peclet number is high. However, the hybrid differencing does not solve the false diffusion problem, while setting diffusion to zero for not so high Peclet number (|Pe| > 2) could turn to be problematic.

Therefore, in order to have a formulation as faithful to reality as possible, this study will be done by using the upwind scheme, which allows instead to take into consideration convection also when its contribution is not very strong.

Once that the equation has been written as a function of the property in the various nodal point, depending on the scheme, it is possible to group the various coefficient in a way that the discretized equation can have the general formulation:

$$a_p\Phi_p = a_t\Phi_t + a_b\Phi_b + a_n\Phi_n + a_s\Phi_s + a_w\Phi_w + a_e\Phi_e + S_u \qquad (2.9)$$

with

$$a_p = a_t + a_b + a_n + a_s + a_w + a_e - \Delta F - S_p \qquad (2.10)$$

It is interesting to notice that whatever the scheme, the source term described in Eq. 2.6 can cause instabilities in the program, due to the boundedness condition for stability. In order to avoid this problem, the term is divided: the positive terms are added in the S_u term, which is added on the right of Equation 2.9, while the negative terms are added in the S_p term, which, on the other hand, is subtracted to the a_p term, as shown in Equation 2.10.

2.2 Modelling categories

In the fluid dynamic modelling practice, and in particular for fluidized bed, three main modelling categories can be individuated: the empirical, the semi-empirical and the CFD approach.

[3] The Peclet number is the ratio between the convective mass flux and the diffusion conductance at cell face, i.e. it is a measure of the relative relevance of convection vs diffusion. Hence a high Peclet number indicates convection-dominated fluxes while a low Peclet number suggests a highly diffusive flux.

The empirical approach, usually adopted for the investigation of specific phenomena, is based on empirical correlations and often on trial and errors procedures, which makes the scale up risky. Despite this and the fact that this approach provides little mechanistic understanding of the studied process, this modelling technique has however widely been used by manufacturers, having a low computational cost and available data from many years of experience (often not accessible to the public).

The semi-empirical approach, that is mostly used for macroscopic processes investigations, in which theory is combined with empirical correlations or with some simplifying hypothesis mainly regarding velocity fields (in order to skip solving the momentum equation). The main advantage of this type of modelling is that it reliably describes fluid-dynamics, combustion and heat transfer at a macroscopic scale keeping a low computational cost, while the main disadvantage is that the scale up it still takes into account some empirical correlation, maintaining a certain risk degree. Finally, the CFD approach, in which the momentum equation is solved, but that results to be very time-consuming and needs high performance machines while still needing validation afterwards, and therefore is mostly used in very focused studies, in order to decrease the computational cost [16].

The approach used in this study is semi-empirical, i.e. the mass balances are solved, while instead of solving the momentum equation for the velocity fields some simplifications have been used. In order to obtain the velocity fields for both gas and solids, it has been used the potential flow approach, described by the following:

$$\nabla(-D\,\nabla\Phi) = \sum_{n} S_n \tag{2.11}$$

In which the diffusion conductance at the cell face can be an arbitrary value and Φ is the potential function. In this part of the calculation also the gas and solid densities can be set to an arbitrary value, and the initial velocities are set to zero.

It is important to notice that this approach takes into account only the diffusion contribution in the transport equation, and for the gas in the first iteration also the source term is set to zero, while in the others will account for the gas generation and/or consumption due to non-equimolar reactions, while is always set to zero for the solids as no volumetric solids generation is considered. The equations taken into account for the gas and the solid potential function are as follows, respectively:

$$\frac{\partial}{\partial \vec{\mathrm{r}}}\left(\mathrm{D}\frac{\partial \Phi \mathrm{g}}{\partial \vec{\mathrm{r}}}\right) + \dot{\mathrm{n}}''' = 0 \tag{2.12}$$

$$\frac{\partial}{\partial \vec{r}}\left(\mathrm{D}\frac{\partial \Phi \mathrm{s}}{\partial \vec{r}}\right) = 0 \tag{2.13}$$

The equation is solved for the general variable Φ, which once converges is then used to calculate the gas and solids velocity respectively as in (2.13) and (2.14):

$$u_g = \frac{RT}{p}\left(D\frac{\partial \Phi \mathrm{g}}{\partial \vec{r}}\right) \tag{2.13}$$

$$u_s = \frac{1}{\rho_s \varepsilon_s}\left(\Gamma \frac{\partial \Phi s}{\partial \vec{r}}\right) \tag{2.14}$$

The calculated velocities are then used in the mass balances. The method proceeds in a way that after the mass balance has been solved, the mole generation due to non-equimolar reaction found is accounted by updating the source term in Equation 2.12.

3 Code structure and development

The Matlab® code used for the simulations has been structured with a main function that calls the data in input and the generated mesh for the considered boiler, and that solves the potential flow function for the gas and the solids first, and then goes to the mass balance for solids and gases and finally to the heat balance.

While the parts regarding input, meshing and the potential flow functions were formerly implemented, this work will mainly focus on the mass balance for the gases, in which six gas species are considered. The mass balance function is called by the main one, and in turn calls for other functions which account for velocity, boundary conditions, initial values source terms and the solver. In order to handle the high number of cells in the mesh necessary to the accuracy of the solution has been used the TDMA (Tri-Diagonal Matrix Algorithm) solver. The solver is a simplified Gaussian elimination method used for tridiagonal matrices, and its main parts are the forward elimination, in which the coefficients of the systems are modified ad hoc, and the backwards substitution, in which the new coefficients are substituted back to the system. The TDMA solver can be used only for diagonally dominant matrices [17]. Below follows a brief description of how each file has been implemented.

First of all the solving domain is divided into dense bed and freeboard. In the dense bed the gas is in turn divided into emulsion and bubble phase. This last division will be described in detail in Section 3.1.

3.1 The dense bed

The dense bed is located in the bottom of the reactor, where most of the solids are located. The primary gas is injected from below. The gas in the dense bed has been divided into emulsion and bubble phase. The emulsion is the phase in which the reactions happen, while the bubble phase compensates for the flow exceeding or lacking from the minimum fluidization flow. The deviation of the emulsion flow from the minimum fluidization flow can be due to two main reasons: the gas volume generation or consumption due to non-equimolar reactions, and the changing cross-section of the reactor. A continuous mass exchange between the two gas phases will also be considered. The two phases are therefore modelled separately, but considering the previously mentioned exchanges between the two.

The emulsion is the part of the dense bed which particles are at the minimum fluidization velocity. The minimum fluidization velocity can be calculated from the correlation shown in Equation 3.1 below [16], and it is normally a function of the solids particle diameter and density and of the fluid density and viscosity.

$$Re_{mf} = \sqrt{(33.7)^2 + 0.0408 \cdot Ar} - 33.7 \qquad (3.1)$$

Where the Archimedes number is defined as [17]:

$$Ar = \frac{d_s^3 \rho_g (\rho_s - \rho_g) g}{\mu^2} \tag{3.2}$$

Typical values the minimum fluidization Reynolds number for BFB reactors are in the range of 10^{-5} to 10^3. In this work a minimum fluidization velocity value of 5 cm/s is assumed.

The velocity field for the emulsion gas has been taken as purely vertical and equal to the minimum fluidization one, while for the bubble phase the lateral velocity is given by the results of the potential flow function and the vertical is the difference between the total gas velocity and the minimum fluidization one. Vertical diffusion is set to zero in the first layer of the dense bed in order to prevent the gas from flowing back to the inlet, which would result in an outwards diffusive flow.

The initial conditions are given from the initial concentration for each gas species at the bottom inlet (see Table 1). The considered species are typical in combustors, and the initial concentrations have been assumed taking into account an excess of air with respect to the combustibles, and a minimum part of water and carbon dioxide in the inlet.

Table 1: *Gas species considered with respective initial volume concentrations*

Gas species	$[C_i]_{\%vol}$
N_2	0.55
H_2	0.09
CO	0.09
O_2	0.15
H_2O	0.06
CO_2	0.06

The boundary conditions at the outlet of the dense bed are set to a zero concentration gradient, while is a known concentration value for the inlet. Setting the boundary condition means, in Equation 2.9, set to zero the corresponding a-coefficient, however that coefficient reappears in the form of a source term of the type described in Equation 2.6.

Combining Equation 2.3 in 1D, meaning that only the west and east boundary will be considered for simplicity (the derivation is analogous for 3D system), and 2.6, and implementing the substitution, for which the subscript refer to the cell organization presented in Figure 4:

$$F_e \phi_e - F_w \phi_w = D_e(\phi_E - \phi_P) - D_w(\phi_P - \phi_W) + S_u + S_p \Phi_p \tag{3.3}$$

Considering a positive velocity, and therefore a flow going from west to east in both boundary faces, the above equation becomes:

$$F_e\phi_P - F_w\phi_W = D_e(\phi_E - \phi_P) - D_w(\phi_P - \phi_W) + S_u + S_p\Phi_p \quad (3.4)$$

In which the capital letters refer to the neighbouring node and the lower case ones to the boundary faces. Grouping the coefficients of the former equation it is obtained:

$$(F_e + D_e + D_w - S_p)\phi_P = D_e\phi_E + (D_w + F_w)\phi_W + S_u \quad (3.5)$$

Which becomes:

$$(D_e + D_w + F_w + \Delta F - S_p)\phi_P = D_e\phi_E + (D_w + F_w)\phi_W + S_u \quad (3.6)$$

Assuming the general form presented in Equation 2.9:

$$a_p\phi_P = a_e\phi_E + a_w\phi_W + S_u \quad (3.7)$$

Let us assume now that the boundary condition will be imposed at the west boundary, and let us consider the two cases: the known concentration value first and the zero gradient then.

In the first case, the general property ϕ at the western boundary, which from now on will be called A in order to highlight that it is a particular boundary, becomes known, and therefore it will be called ϕ_A and the same will be for the convective and diffusion conductance at that face. Equation 3.4 becomes:

$$F_e\phi_P - F_A\phi_A = D_e(\phi_E - \phi_P) - D_A(\phi_P - \phi_A) + S_u + S_p\Phi_p \quad (3.8)$$

Which is

$$(D_e + D_A + F_A + \Delta F - S_p)\phi_P = D_e\phi_E + S_u + (D_A + F_A)\phi_A \quad (3.9)$$

Where the last term on the right side of the equation is the a-coefficient at the western boundary in the considered A point times the known concentration value in the same point which can be associated in form with S_u, and therefore called ${S_u}^{BC}$, and on the left side the same reasoning can be done with S_p, which will then become ${S_p}^{BC}$, while it can be noticed that the term $a_w\phi_W$ has disappeared. Generalizing, the above mentioned source terms due to the boundary conditions can be written:

$${S_u}^{BC} = a_i\phi_i \quad (3.10)$$

$${S_p}^{BC} = -a_i \quad (3.11)$$

Where *i* is the considered boundary.

Concerning the second case, the concentration gradient is zero, which means that $\phi_W = \phi_P$, Equation 3.4 becomes:

$$F_e\phi_P - F_A\phi_P = D_e(\phi_E - \phi_P) - D_A(\phi_P - \phi_P) + S_u + S_p\Phi_p \quad (3.12)$$

So that the diffusive term at the western boundary becomes zero and the previous becomes:

$$(D_e + \Delta F - S_p)\phi_P = D_e\phi_E + S_u \quad (3.13)$$

In this second case it can be noticed how not only the western boundary term has disappeared, but also that it has not appeared back as a boundary condition source term. Therefore the zero gradient condition translates into:

$$S_u{}^{BC} = 0 \tag{3.14}$$

$$S_p{}^{BC} = 0 \tag{3.15}$$

Concerning the source term definition, a first distinction can be done between the actual source term due to homogeneous reactions between gas species, and other terms representing the gas exchange between bubble and emulsion phases.

A first source term is given by homogeneous reactions, and in particular the following have been considered:

$$H_2 + \frac{1}{2}O_2 \rightarrow H_2O \tag{3.16 a}$$

$$CO + \frac{1}{2}O_2 \rightarrow CO_2 \tag{3.16 b}$$

$$CO + H_2O \rightleftharpoons H_2 + CO_2 \tag{3.16 c}$$

In which reaction 3.16c, which is normally called water gas shift, will be considered as two reactions in turn, one for each direction in which the reaction occurs. Each reaction, according to chemical kinetics, has a speed of reaction, expressed through the reaction rate. From the reaction rate and stoichiometric coefficients the consumption or generation of each gas species can be evaluated, also called homogeneous herein on, S_{hom}. In order to obtain the source term itself in a given cell, the reaction rate must be multiplied by the cell volume.

The expressions for the reaction rates have been taken from [18]. The backward reaction rate of Equation 3.16c can be calculated through the equilibrium constant, being the rates equal at the equilibrium [19]. The rates expressions are shown in Equations 3.17a to 3.17d.

$$r_{H_2} = 1.08 \cdot 10^7 \cdot e^{-\frac{125525}{RT}} \cdot [H_2] \cdot [O_2] \tag{3.17 a}$$

$$r_{CO} = 1.78 \cdot 10^{10} \cdot e^{-\frac{180032}{RT}} \cdot [CO] \cdot [H_2O]^{0.5} \cdot [O_2]^{0.25} \tag{3.17 b}$$

$$r_{WGSR\rightarrow} = 0.2778 \cdot e^{-\frac{12560}{RT}} \cdot [CO] \cdot [H_2O] \tag{3.17 c}$$

$$r_{WGSR\leftarrow} = 3.2891 \cdot e^{-\frac{34730}{RT}} \cdot [CO_2] \cdot [H_2] \tag{3.17d}$$

Hence, for each gas species, the homogeneous source term will be the sum of the above mentioned term for each reaction in which the species is involved.

The source term expressing the general gas transfer from the bubble phase to the emulsion phase is described by equation 3.18 [20]:

$$S_{exch,em} = K_{be}([C_i]_{bub} - [C_i]_{em}) \cdot V \tag{3.18}$$

while for the bubble phase has the opposite sign.

K_{be} is the transfer coefficient between the emulsion and bubble phase, and it can be calculated using the correlation in Equation 3.19 [21]:

$$K_{be} = 4.5\left(\frac{u_{mf}}{d_{bub}}\right) + 5.85\left(\frac{Dg^{0.5}}{d_{bub}^{2.5}}\right)^{0.5} \tag{3.19}$$

It can be noticed that the exchange coefficient decreases with the increase of the bubble diameter, which is turn varies with the boiler's height [22]. In this treatise will be used the correlation proposed by Darton et al. (1977):

$$d_{bub} = 0.54\frac{\left(u_g - u_{mf}\right)^{0.4}}{g^{0.2}}\left(z + 4\sqrt{\frac{A_{bed}}{n_{nozzle}}}\right)^{0.8} \tag{3.20}$$

In which a normal value for the ratio between the bed area and the number of nozzles in the fluidization grid is 0.01 m^{-2}.

Normal values for the transfer coefficient are between 1 and 10 s^{-1}, but those values have been found for small-scale combustors, while no experimental data is found in literature for large-scale plants. It has been estimated however that the coefficient should decrease with the reactor dimensions increase, which should lead to a range of 0.1-1 s^{-1} [23]. For simplicity, most of the simulations will be run using a constant value set to 1 s^{-1}. However, being this coefficient one of the sensitive parameters subject of study in this work, it will be then changed, using the height dependency instead, according to Eqs. 3.19 and 3.20, using a diffusivity factor of $22 \cdot 10^{-6}\ m^2/s$ [24]. This value has been validated by making sure that the resulting exchange coefficient was within the range suggested from the literature [25].

Since the cells do not generally have a regular size, the area in the bottom of the cell can be different than that in the top face, but as the volumetric flow must remain constant, a third source term contribution must be added. This term is such that the flow needed or in excess in the emulsion phase is compensated by the bubble phase. An example of the calculation of such term from the bubble to the emulsion phase is given in Equation 3.21, in which it is assumed that an enlargement of the cross sectional area in the flow direction.

$$S_{exp/contr} = u_{mf}(A_t - A_b)[C_i]_{bub} \tag{3.21}$$

It is clear that also this term, like the one formerly described, must be the same and with opposite sign for the other phase, being these terms only of exchange between phases and not actual source terms.

Lastly, one last term accounts for the exchange between phases due to the gas volume generation or dissipation by non-equimolar reactions (Equations 3.16a and 3.16b). The principle is then the same as in Equation 3.18, so when gas is consumed in a phase, the bubble provides the lost quantity and vice versa if moles are generated in the emulsion.

Equation 3.22 shows the term in the mass balance for the emulsion, while for the bubble phase the term will be exactly the same but with opposite sign.

$$S_{react,exch} = \sum_{i=1}^{N_g} \Delta\dot{n}_i \, [C_i] \tag{3.22}$$

Where $\Delta\dot{n}_i$ is the net mole generation or consumption for each considered reaction.

Convergence is first evaluated in each gas phase, in order to completely decouple each code section, making also easier to individuate possible errors and to make changes when needed, then a total convergence in calculated. An absolute and relative error have been defined in order to evaluate convergence:

$$err_{abs} = S_{in} + S_{gen} + S_{out} \tag{3.23}$$

$$err_{rel} = \frac{|err_{abs}|}{|S_{in}| + |S_{gen}|} \tag{3.24}$$

In which the flows in the absolute error calculation are taken with their respective signs. The ideal convergence in the dense bed is achieved when the sum of what is injected and what is generated inside the domain equals the outgoing flow. The real convergence uses a tolerance value for the relative error of 10^{-3}.

3.2 The freeboard

In the freeboard the gas flow is considered single-phased. Therefore the initial inlet values must be calculated as a weighted concentration average of the two-phased gas flow exiting the dense bed. In particular, taking into account that in both the cells before and after the border between the two diffusion is set to zero, the concentration at the freeboard inlet is calculated imposing continuity, i.e. for each gas species:

$$\left(F.b_{freeboard}\Phi_{freeboard}\right)_{nz+1} = (F.t_{bub}\Phi_{bub})_{nz} + (F.t_{em}\Phi_{em})_{nz} \tag{3.25}$$

In which nz is the node right below the dense bed/freeboard border, and $nz + 1$ the one right above the border, as schematically shown in Figure 5 below.

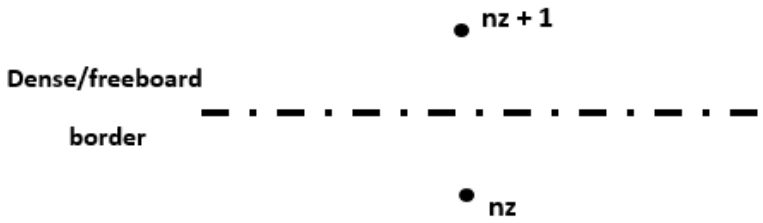

***Figure 5**: Schematic representation of the nodes' organization at the border of the dense bed and freeboard domains*

The velocity field in the freeboard, on the other hand, is given by the velocity field found with the potential flow function. As in the dense bed, zero diffusion is assumed in the first layer of the domain in order to decouple the two zones.

Concerning initial and boundary conditions, as well as the source terms, it can be applied the same reasoning as in the dense bed, with the difference that here the gas is again considered single-phased. For this same reason the source term is now only the one due to homogeneous reactions. Convergence is defined in a similar way as in the dense bed.

Once both dense bed and freeboard mass balances have reached convergence, the source term in the potential function for the gases, Equation 2.9, is updated and the velocity fields recalculated. Then the mass balance is solved again, until global convergence is reached.

4 Simulations

The main goal of this work is to investigate the influence of a reactor's upscaling on the combustion performance, and in particular the typical combustion pattern in a large-scale biomass boiler, where the volatile release occurs in one portion of the cross-sectional area while air is in the rest of it. The influence of the inlet gas velocity, the gas exchange coefficient (Eq. 3.19), the height of the dense bed and the lateral diffusion coefficient are studied. For simplicity, the simulations are run in BFB mode.

4.1 Reactor's geometry and assumptions

The geometry of the reactor can be observed in Figure 6, as well as the meshing grid. It can be clearly seen how the cross sectional area changes with the height. The reactor's outlets (highlighted in red) are located on the north wall. The fuel inlets, six in total, are instead positioned within the first five meters from the air inlet ($z = 0$), four on the south wall and two on the north wall. Although the fuel feeds are originally placed in the freeboard, the injection points have been moved to the dense bed in order to study the behaviour of devolatilizing fuel particles (which are coarse and thus often populate the dense bed after being fed to the unit).

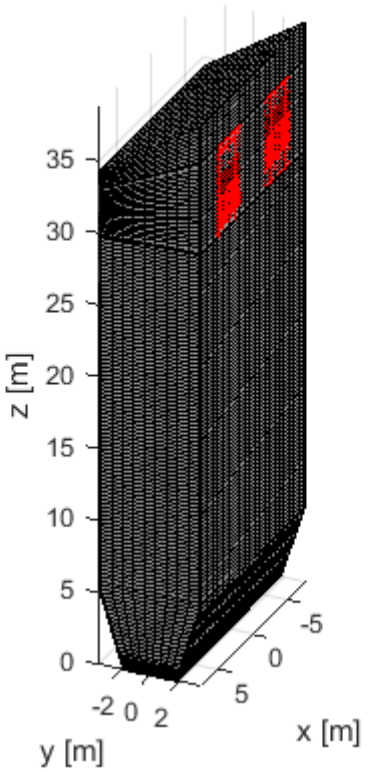

***Figure 6**: Geometry and mesh of the considered reactor*

Many fuel feeding in conventional and FB boilers are located on one side of the reactor's bottom. Due to the fast kinetics of combustion, in these conditions the fuel burns almost instantly very close to the feeding, and the conditions change with the inlet velocity. Particularly, the volatiles will be fed from the south side of the inlet area, taking into account that most of the fuel feeds are located on the south wall. The injection area has been calculated bearing in mind that the inlet velocity for both the volatiles and air must be the same.

The conditions of lateral injection have been inserted as boundary conditions, and in particular limiting the entrance of H_2, CO, H_2O and $CO_2$to the above mentioned area portion, while in the remaining inlet area combustion air has been injected. Illustrative sketch in Figure 7.

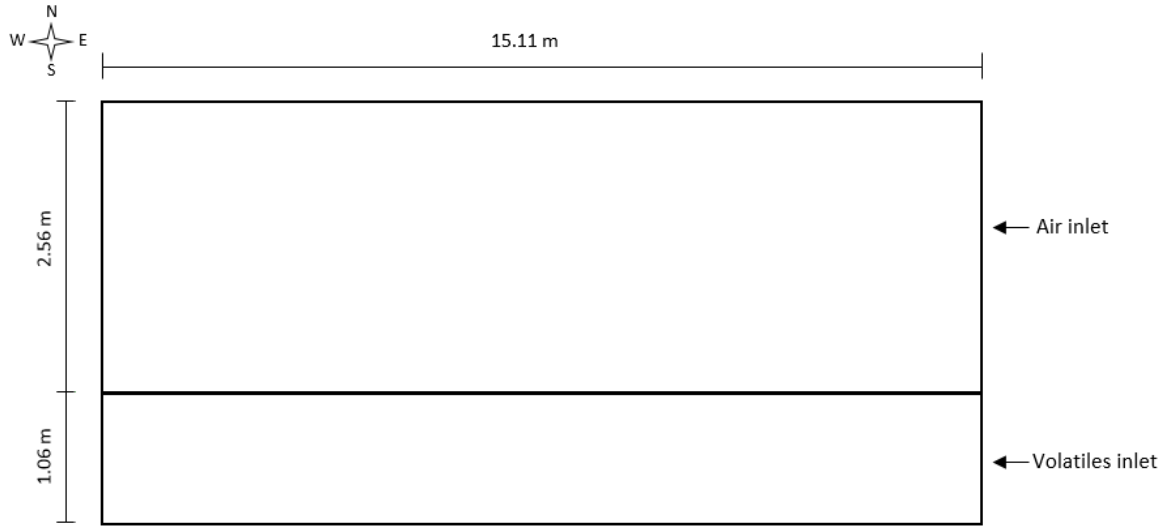

***Figure 7**: Schematic of the injection area separation*

Referring to Table 1, which reports the total concentrations as if the species were homogeneously injected in the whole area, once the division has been done, there will be different local values of initial concentration depending on the injection area, which will be the ones shown in the results chapter, and that are shown in Table 2 and 3 respectively for air and for volatiles.

***Table 2**: Air concentration at the combustor inlet*

Gas species	$[C_i]_{\%vol}$
N_2	0.79
O_2	0.21

***Table 3** : Volatiles concentration at the combustor inlet*

Gas species	$[C_i]_{\%vol}$
H_2	0.3
CO	0.3
H_2O	0.2
CO_2	0.2

4.2 Studied parameters

In Table 4 the simulated cases for this study are summarized.

***Table 4** : Analysed cases summary*

Case	u_0 $[m/s]$	K_{be} $[s^{-1}]$	H_b $[m]$	$D_{g,lat}$ $[m^2/s]$
1	3.5	1	0.38	0.1
2	1	1	0.38	0.1
3	5	1	0.38	0.1
4	3.5	$\propto f(z)$	0.38	0.1
5	3.5	$\propto f(z)$	0.8	0.1
6	3.5	1	0.38	0.01
7	3.5	1	0.38	1

Three values of inlet velocity will be considered, starting from a reference value of 3.5 m/s, maintaining constant the dense bed height and the gas exchange coefficient. Thereafter the gas exchange coefficient is studied considering its dependence with height. Thereafter the dense bed height will be changed, and finally, the gas lateral diffusion coefficient.

The diffusion coefficient is a constant describing the proportion between the molar flow due to diffusion and the concentration gradient in one direction, as described by Fick's law [25]:

$$D_r = \frac{-f_{i,r}}{\partial C_i / \partial r}$$

In this study the gas lateral diffusion coefficient will be changed, which means in x and y directions, while the axial will remain fixed. Therefore it will be changed the rate at which the gas flow will move through the lateral faces of the cell.

5 Results and discussion

This chapter shows the results of the simulations described in Chapter 4, with particular focus on the gases concentrations and the exchange rate when interesting. It has also been observed what happens to the velocity of the gases when approaching the top exit, which is located in the south face of the boiler and yields singularities.

After discussing the reference case, the results are classified into four subsections: gas velocity, effect of a varied gas exchange factor, effect of a varied dense bed height and effect of a varied lateral gas dispersion.

5.1 Reference case

In order to give a better idea of how the furtherly considered parameters affect the performance of the reactor, the results below will be shown in the most detailed way possible. This means that concentrations and velocities will be displayed in the almost totality of the reactor's length, so that any sensitive change can be easily pointed.

Figures 8 to 12 below show the concentration distribution of each gas species for five different values of reactor's heights. That greater focus has been given to the inlet layers for the consumed species (i.e. H_2, CO and O_2), and to the outlet layers for the generated ones (i.e. CO_2 and H_2O), while nitrogen, being inert, is not shown. Note that the x axis displayed herein on in the figures and called y (it is the y-axis in Fig. 6) is the north-south view of Figure 7, being of interest how the species mix between the two injection areas.

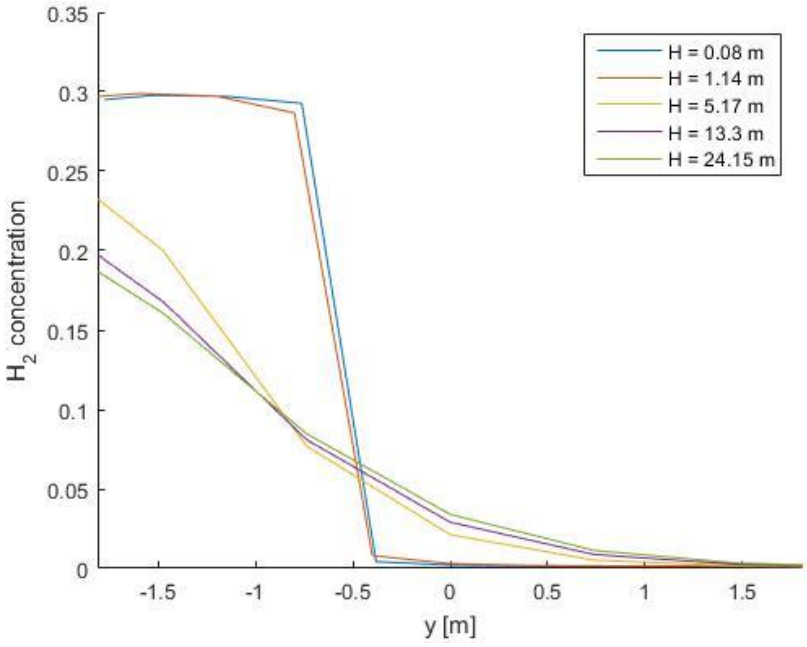

***Figure 8**: Lateral distribution of H_2 concentration at several heights*

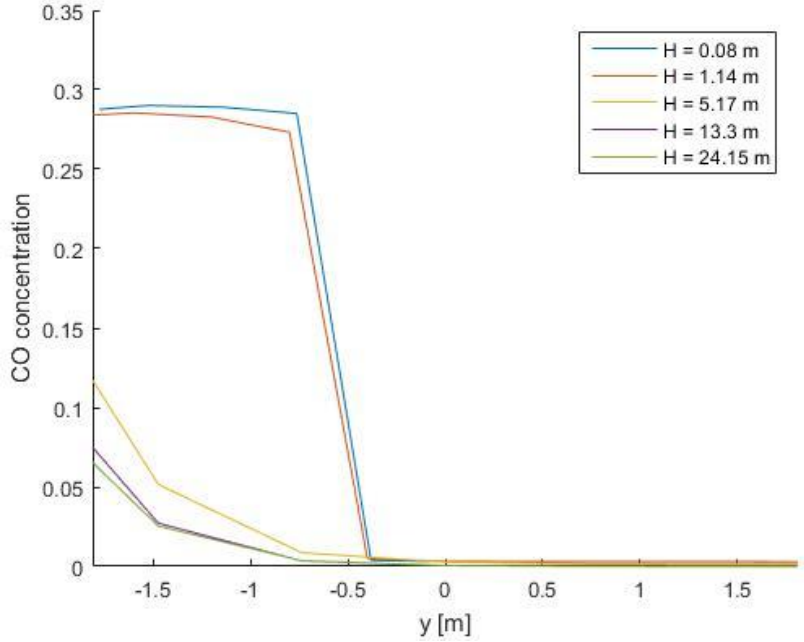

***Figure 9**: Lateral distribution of CO concentration at several heights*

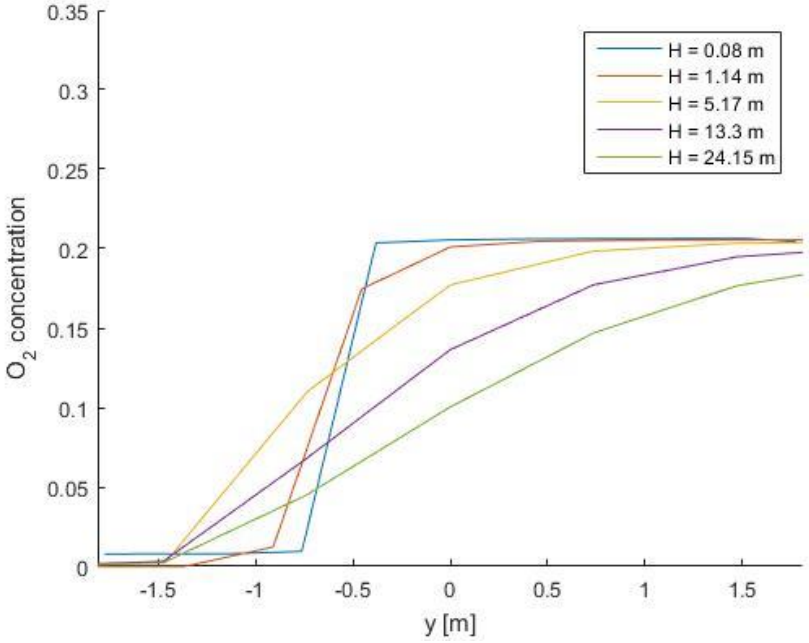

***Figure 10**: Lateral distribution of O_2 concentration at several heights*

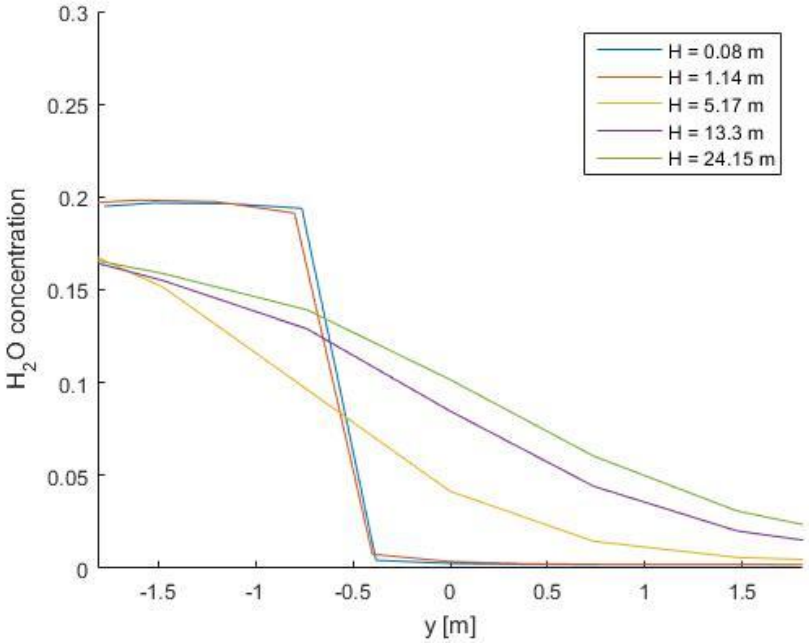

***Figure 11**: Lateral distribution of H_2O concentration at several heights*

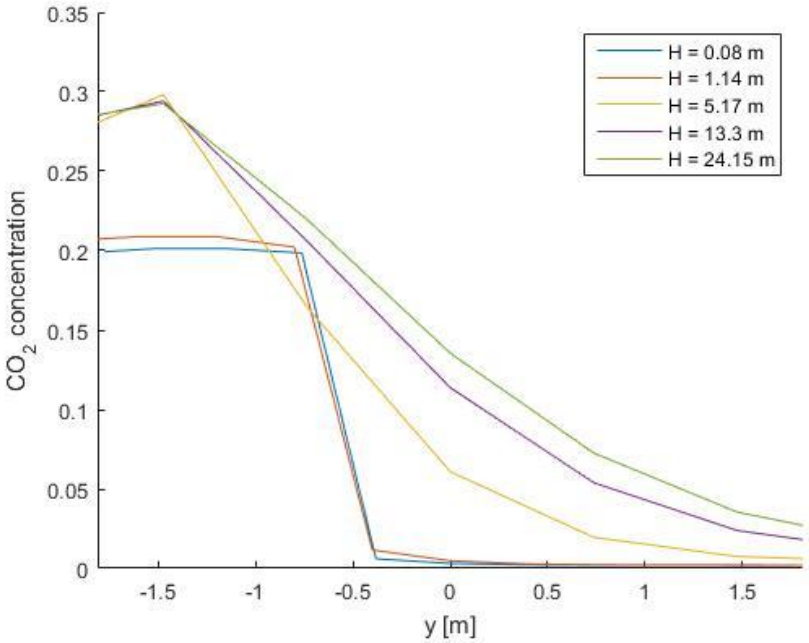

***Figure 12**: Lateral distribution of CO_2 concentration at several heights*

Keeping in mind that volatiles are injected over the left-sided first ~1 m, it can be observed that hydrogen and carbon monoxide do not vary much in concentration in the air inlet side (on the right of the plot) while decreasing fast on the left side. The latter in particular decreases very steeply, reaching much lower concentrations at the reactor's end. This might sound counter intuitive, it is however due to the dependence of the carbon monoxide oxidation' reaction rate from the water concentration (Eq. 3.16 b) which keeps increasing along the boiler's height. In fact, at the reactor's exit, the water concentration is quite high (it can reach up to three times its initial value), being a combustion product, which makes the above mentioned reaction faster in the last stages of the reactor. Oxygen, on the other hand follows a more gentle variation, being it consumed with a proportion of 1:2 with respect to H_2 and CO (see Eqs. 3.16 a and 3.16 b). Finally, the two species generated from hydrogen and carbon monoxide oxidation tend to spread over the cross sectional area along the height.

5.2 Velocity fields and concentrations at the outlet

The velocity is fairly homogeneous over the cross section until the flow reaches the exit area, which, being collocated on the north wall, creates an asymmetry. In Figure 13 such distribution can be appreciated.

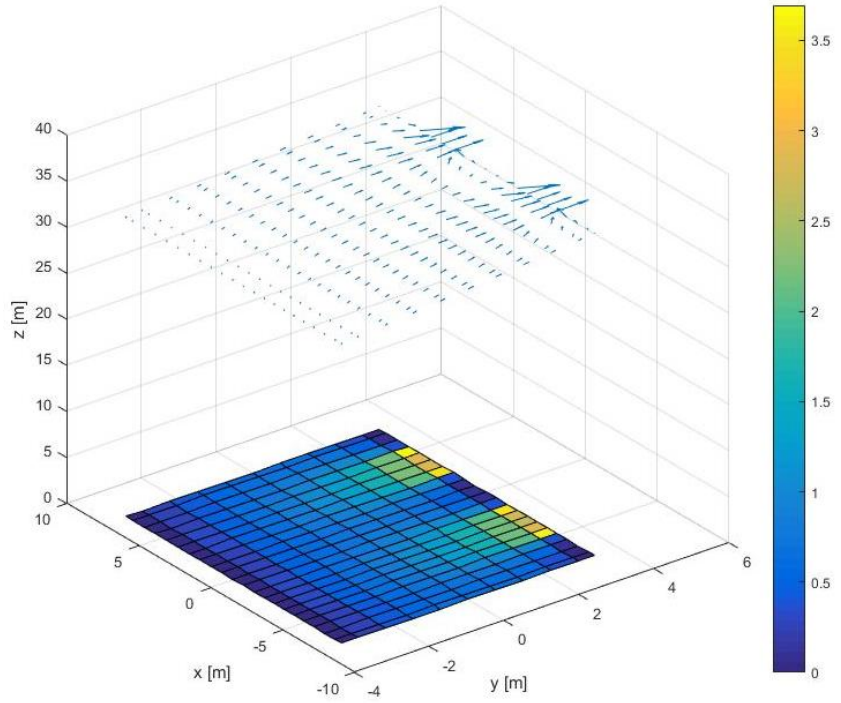

***Figure 13**: Gas velocity distribution at the reactor's height of 35 m*

It is also interesting to observe the concentrations of the combustible species at the exit of the combustor, in order to see which of the two governing mechanisms of combustion, kinetics or mixing, is the responsible of the unburnt at the outlet. The following figures are taken at the height of 32.5 m, which represents a height location in the middle height of the exit ducts (see Fig. 6).

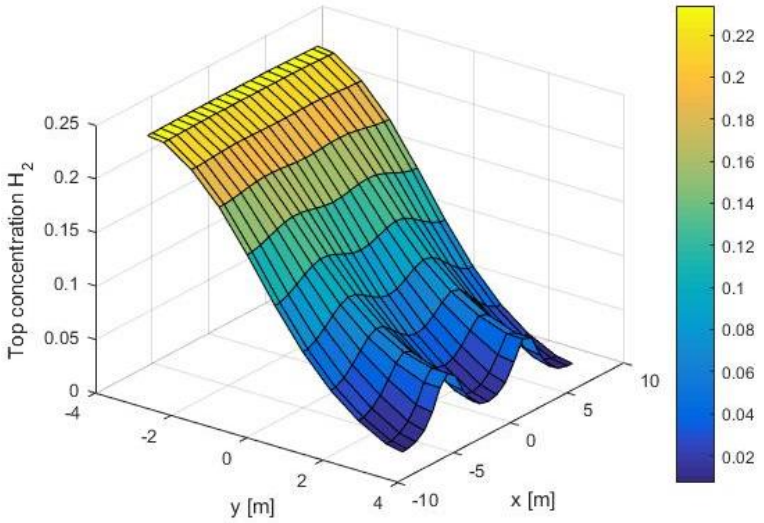

***Figure 14**: Cross-sectional distribution of H_2 concentration at 38.5 m*

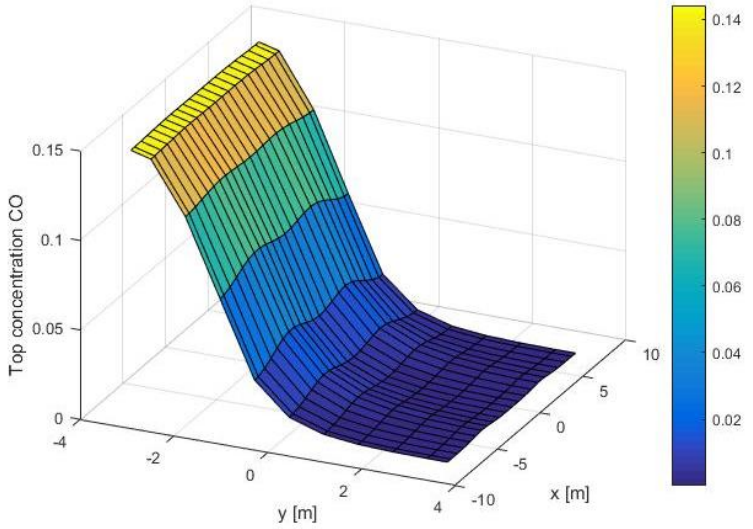

***Figure 15**: Cross-sectional distribution of CO concentration at 38.5 m*

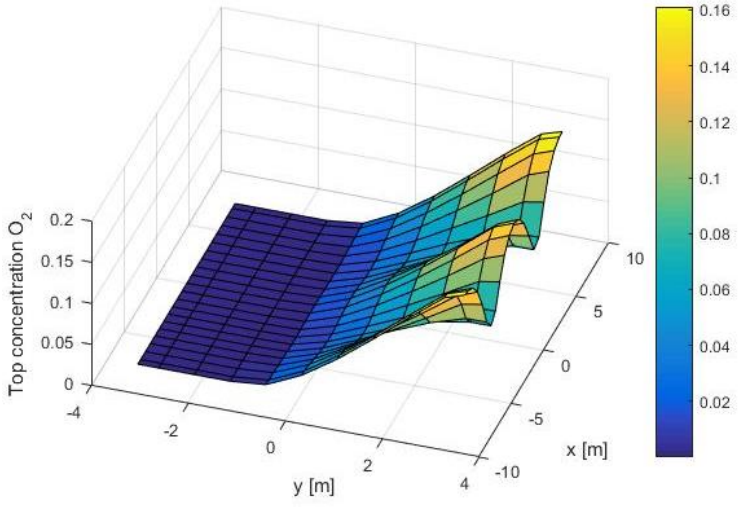

***Figure 16**: Cross-sectional distribution of O_2 concentration at 38.5 m*

It can be seen from comparing Figure 14 and 16 that there is an area in which H_2 and O_2 overlap, but that there is still some unburnt H_2, which means that there is mixing, and that the problem is attributable to kinetics, which happens in a much lighter way for CO (Fig. 15), due to the high water content at that height, which accelerates CO oxidation (see Eq. 3.17b).

5.3 Influence of inlet gas velocity

The inlet velocity has been modified as one of the sensitivity parameters. In particular, two values have been chosen to be respectively 33 % lower and higher than the one in the reference case. While the first two profiles do not change significantly in both cases, although the first two curves in Case 2 start decreasing much closer to the left, which suggests that the oxidation is happening in a broader area, see Figure 17 for CO, it is visible the difference for the upper part of the reactor, and in particular is visible that in the case with higher velocity, the concentration at the same height is higher than the one in the low velocity case. This is due to a better mixing and higher residence time allowed by the lower velocity, while the profiles in the higher velocity case result steeper and more bounded to the injection areas.

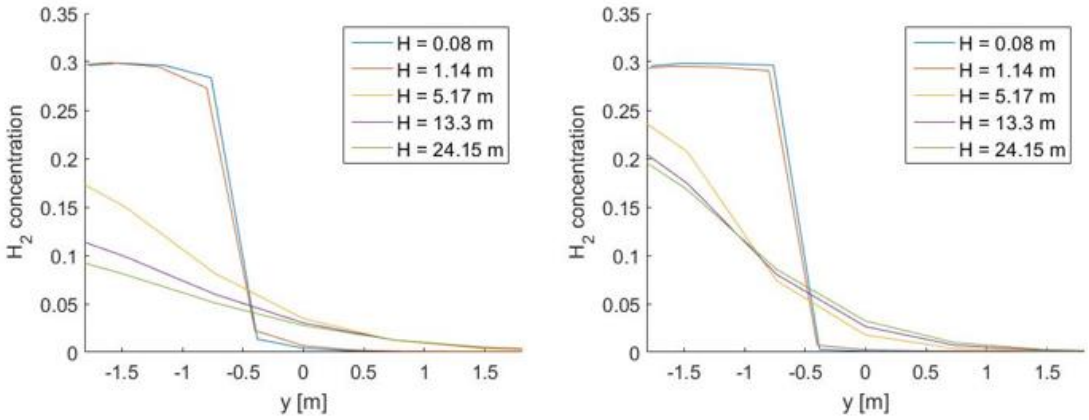

***Figure 17**: Lateral distribution of H_2 concentration at several heights. a) Case 2 (u= 1 m/s), b) Case 3 (u= 5 m/s)*

Also oxygen shows the same trend, in particular it is easy to notice the substantial difference between the two curves for the third considered height. In Case 2 the difference between the line before and the considered one is much bigger than in Case 3, where the concentration on the right asymptotically approaches the initial concentration value, in a very similar way as in the reference case (see Fig. 10). The above mentioned results are shown in Figure 18.

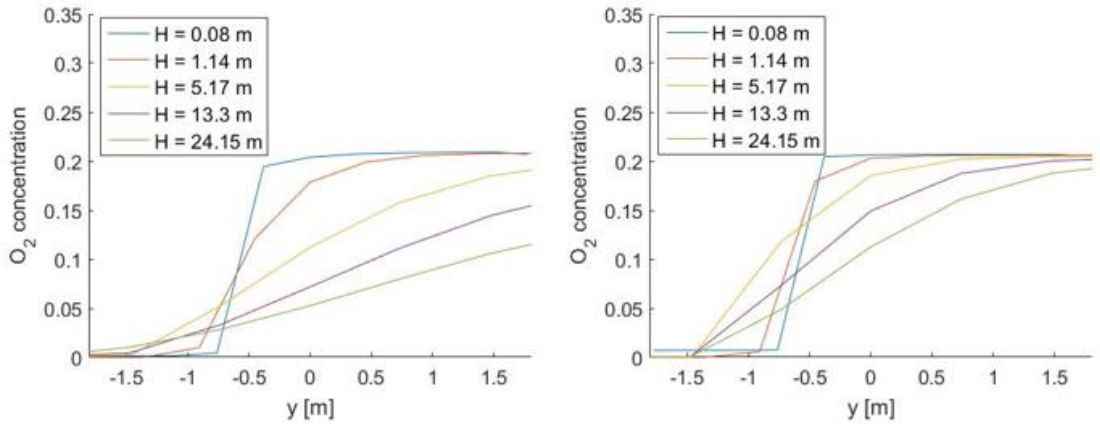

a) b)

Figure 18: *Lateral distribution of O_2 concentration at several heights. a) Case 2 (u= 1 m/s), b) Case 3 (u= 5 m/s)*

For the generated species, H_2O for example in Figure 19, the difference is hardly noticeable and mainly involves the distribution of the species along the separation area in the upper part of the boiler. In fact the curves in the upper part of the reactor are quite flat, which suggests a good distribution of the product species.

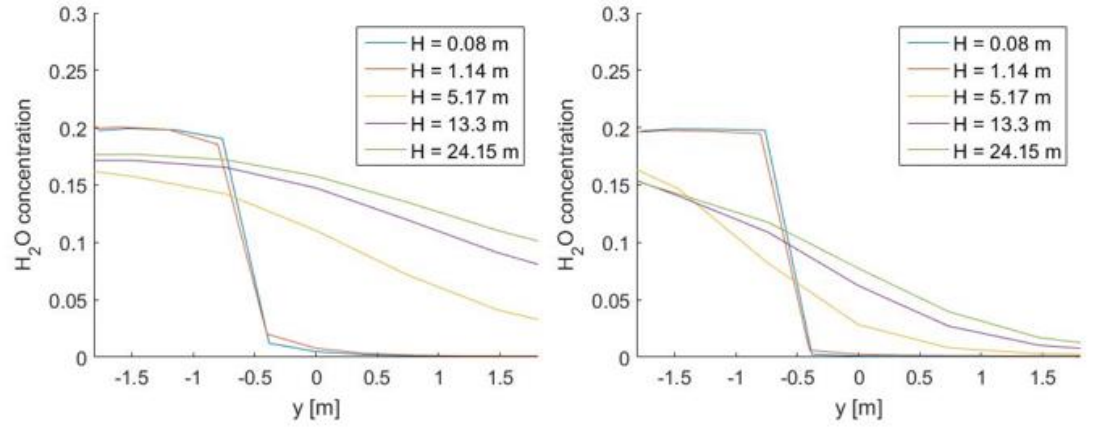

a) b)

***Figure 19**: Lateral distribution of H_2O concentration at several heights. a) Case 2 (u= 1 m/s), b) Case 3 (u= 5 m/s)*

It is visible from the figures above that in the slower case, and especially in the first considered height, the profile is very moved to the injection boundary. This because with lower velocity the oxidation of the species will happen very close to the boundary between the volatiles and the air flows. This phenomenon reflects also in the more even distribution of products along the y-axis with the increasing of z.

As a good measure of the combustion efficiency, Figure 20 shows the total amount of oxygen leaving the outlet area as a function of the inlet gas velocity, which is indicative of the combustion efficiency inside the reactor. As clear from the graph, the unburnt oxygen at the reactor's outlet grows in a parabolic way with the inlet velocity.

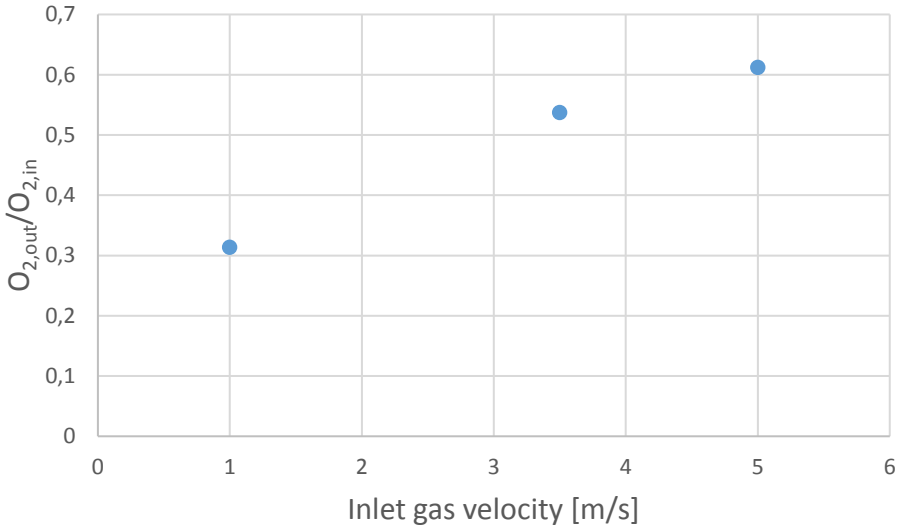

***Figure 20**: Normalized O_2 flow leaving the combustor with respect to the inlet velocity value*

5.4 Exchange coefficient

As clearly understandable from Equations 3.19 and 3.20, keeping the gas exchange coefficient constant, although reasonable in first approximation, is not very accurate, especially when investigating the effect of a consistent dense bed height change, as it will be done in section 5.5. When comparing the global results from this scenario to the reference case, no appreciable difference can be observed in the vast majority of the considered species for the dense bed height of 0.38 m. An example is H_2 (given in Figure 21).

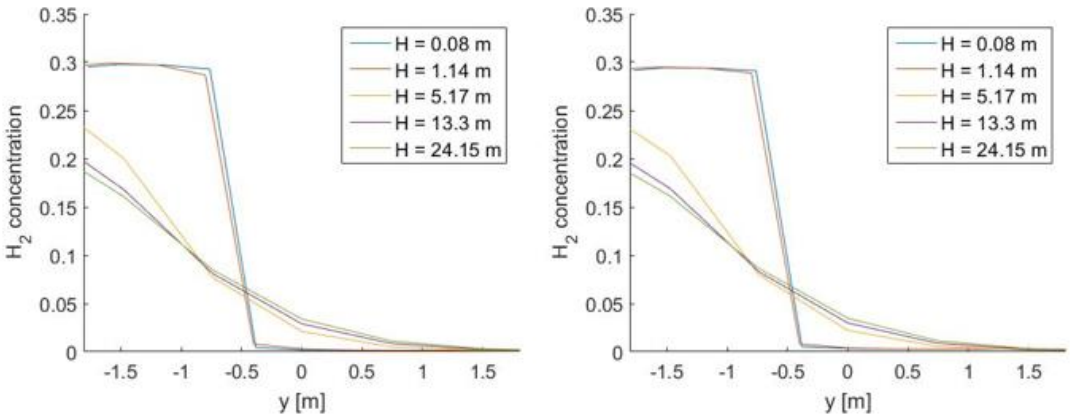

***Figure 21**: Lateral distribution of H_2 concentration at several heights. a) Case 1 (K_{be}= 1 s^{-1}), b) Case 4 (K_{be}= f (z))*

It is interesting, however, to look at the dense bed particularly, since, being it only a small portion of the total reactor's height, the difference could not be visible in such a big scale. In Figure 22 are shown the concentration distributions for H_2 but considering now five different heights all within the dense bed, where the K_{be} is an actual influencing parameter.

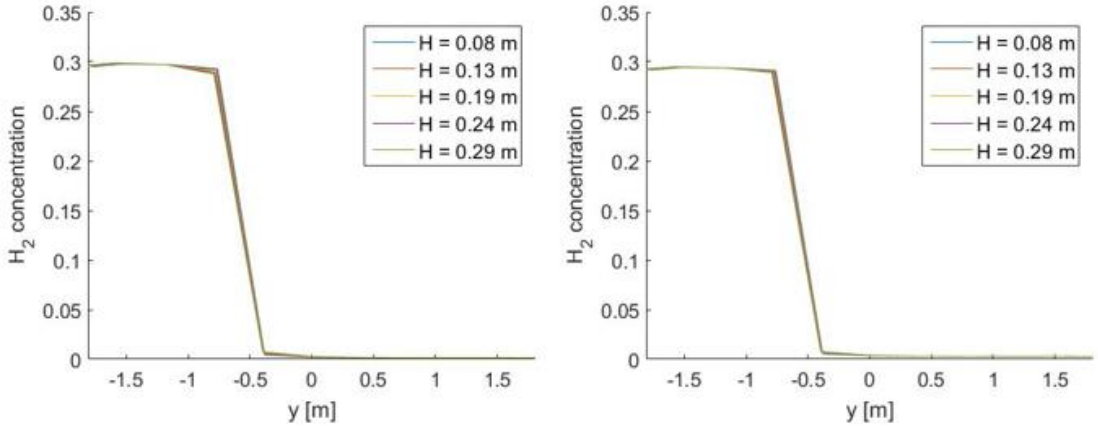

a) b)

***Figure 22**: Lateral distribution of H_2 concentration at several heights within the dense bed. a) Case 1 (K_{be}= 1 s^{-1}), b) Case 4 (K_{be}= f (z))*

Also considering only the dense bed the distribution does not change in an appreciable way, trend that is shared with the other gas species. Note that in the dense bed, the exchange factor is varying within a range of 1.05 and 0.66, with respect to the earlier supposed constant value of 1 s^{-1}.

5.5 Dense bed

Maintaining the gas interphase exchange coefficient variable with height it has been studied how the dense bed height affects the exchange and therefore the concentrations profiles. The value has been set to more than the double of the former, in a way that if said height is an influencing parameter it should be visible from the results.

The same comparison as in the former section has been made. The behaviour is again the same when considering the total reactor's height (see Fig. 23 showing the difference for oxygen concentration).

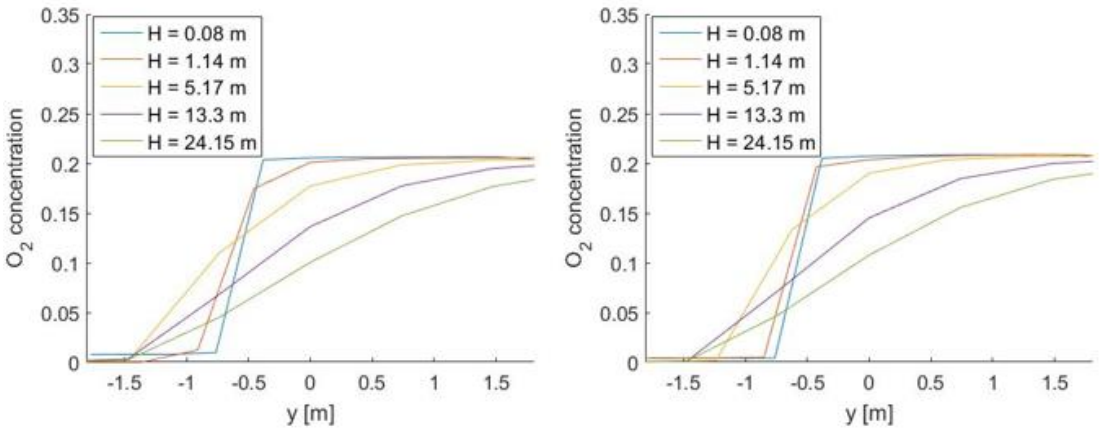

a) b)

***Figure 23**: Lateral distribution of O_2 concentration at several heights. a) Case 1 (H_{db}= 0.38 m), b) Case 5 (H_{db}= 0.8 m)*

Narrowing the observed range to the dense bed, which now will have different dimension, with consequent higher number of considered heights in Case 4 (the same as Case 1 plus some others to cover to whole height), the trend is not changing considerably, but the curves only shift to the left with the height, as shown in Figure 24.

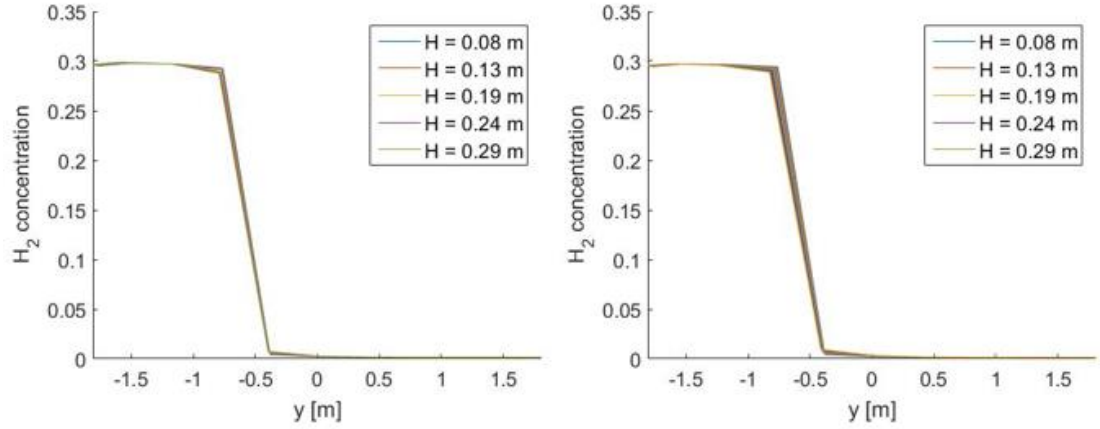

a) b)

***Figure 24**: Lateral distribution of H_2 concentration at several heights within the dense bed. a) Case 1 (H_{db}= 0.38 m), b) Case 5 (H_{db}= 0.8 m)*

In this case the exchange factor is varying within a range of 1.05 and 0.42 s-1, which is much broader than the previous one and, especially in the last part of the dense bed, very far from the previously supposed value of 1 s-1.

5.6 Lateral diffusion coefficient

After setting the parameters back to the reference case conditions, the lateral diffusion coefficient has been decreased to the value of $10^{-2}\ m^2/s$ first and to $1\ m^2/s$ then (respectively Case 6 and 7 in Tb. 2).

It is expected in this case a higher separation between the injection areas for the low diffusion coefficient value, and better spread curves for the high value. All the considered species follow this path, with very steep curves close to the injection boundary in the first layers of the reactor and with less steep curves at higher heights, but still presenting a clear separation between the injection areas (for Case 6), while for Case 7, except from the first reactor's layers, the curves adopt a more even distribution along the separation area. Figures 25 and 26 show the concentration distributions for H_2 and CO_2, respectively, in both the considered cases, which can be in turn compared with Figures 8 and 12 for the base case in Section 5.1.

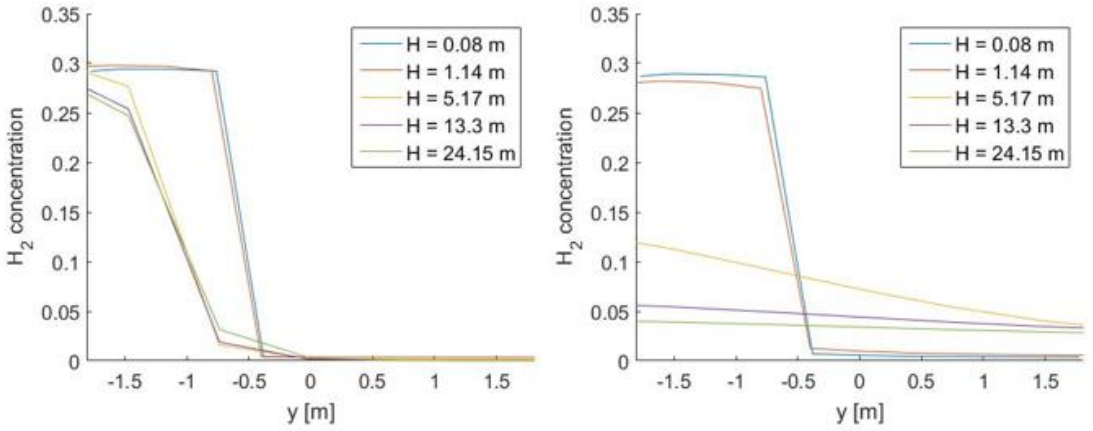

***Figure 25**: Lateral distribution of H_2 concentration at several heights. a) Case 6 (D_{lat}= 10^{-2} m^2/s), b) Case 7 (D_{lat}= 1 m^2/s)*

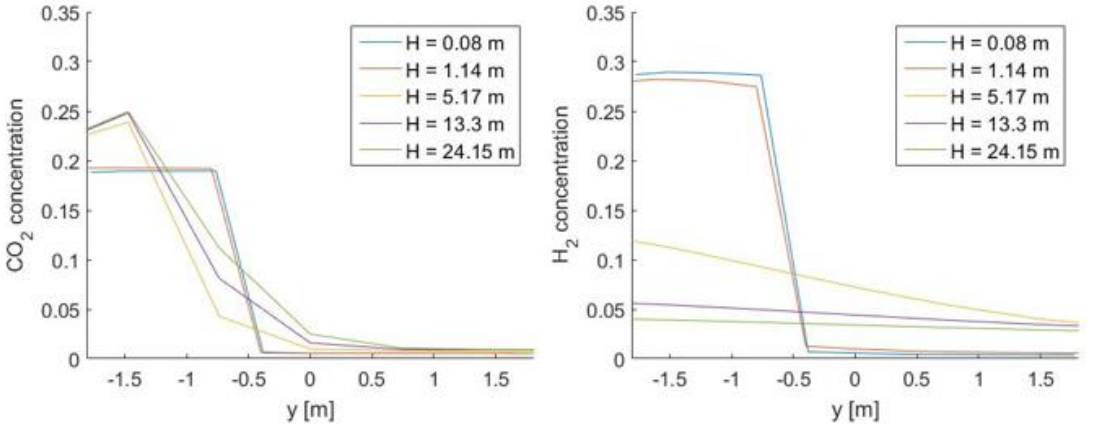

***Figure 26**: Lateral distribution of CO_2 concentration at several heights. a) Case 6 (D_{lat}= 10^{-2} m^2/s), b) Case 7 (D_{lat}= 1 m^2/s)*

In the case of high diffusion coefficient a better mixing is achieved, according to the expectations. In fact, all the gas species spread evenly in the lower half of the reactor's height, and the unburnt for H_2 is minimized with respect to Case 2, which represented the minimum so far. CO, whose concentration was very close to zero at the boiler's outlet for Case 2 is also nearly zero in this case, but the minimum value is reached already at the third considered boiler's height, while in the former the minimum is achieved only in the last considered height. This last comparison can be seen in Figure 27, while Figure 28 shows H_2 distribution at one reactor's height for Case 1, 6 and 7.In the latter particularly is appreciable the difference in behaviour between the three values of lateral diffusion coefficient, with the curve becoming completely flat for the higher value, while maintaining almost a complete separation between injection areas in the lower one.

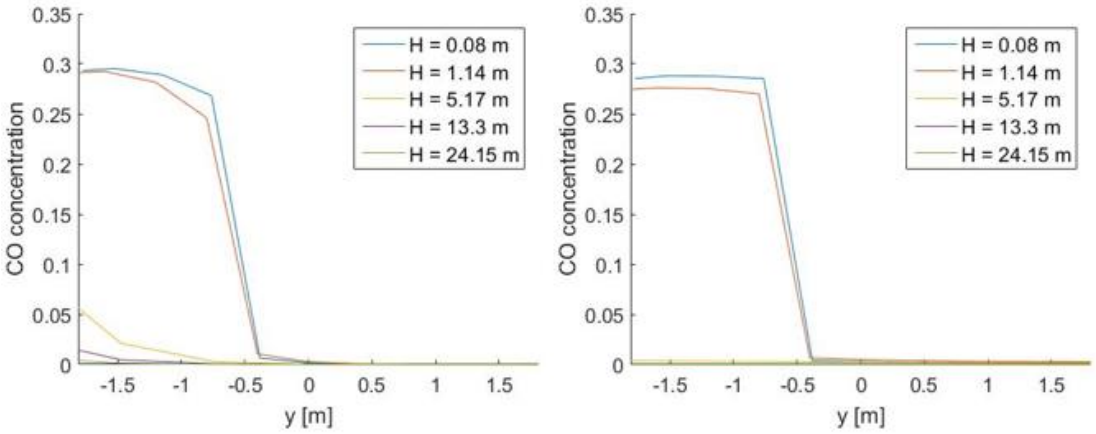

***Figure 27**: Lateral distribution of CO concentration at several heights. a) Case 2 (D_{lat}= 0.1 m^2/s, u=1 m/s), b) Case 7 (D_{lat}= 1 m^2/s, u=3.5 m/s)*

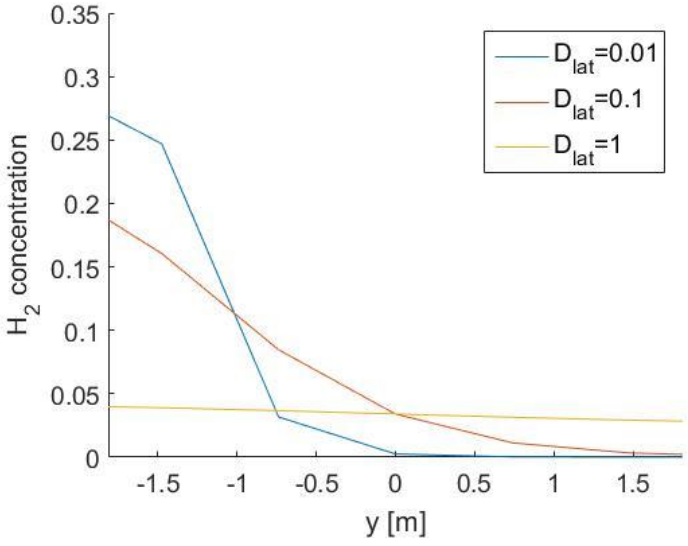

***Figure 28**: H_2 concentration distribution for the emulsion phase at 29.6 m for the three values of diffusion coefficients*

Lastly, similarly to what done at the end of Section 5.3, a comparison between the combusted oxygen depending on the lateral diffusion coefficient has been done at this point again. The comparison is therefore between the reference case and the low and high diffusion coefficients. Figure 29 below shows the unburnt oxygen at the outlet of the boiler's for Cases 1, 6 and 7.

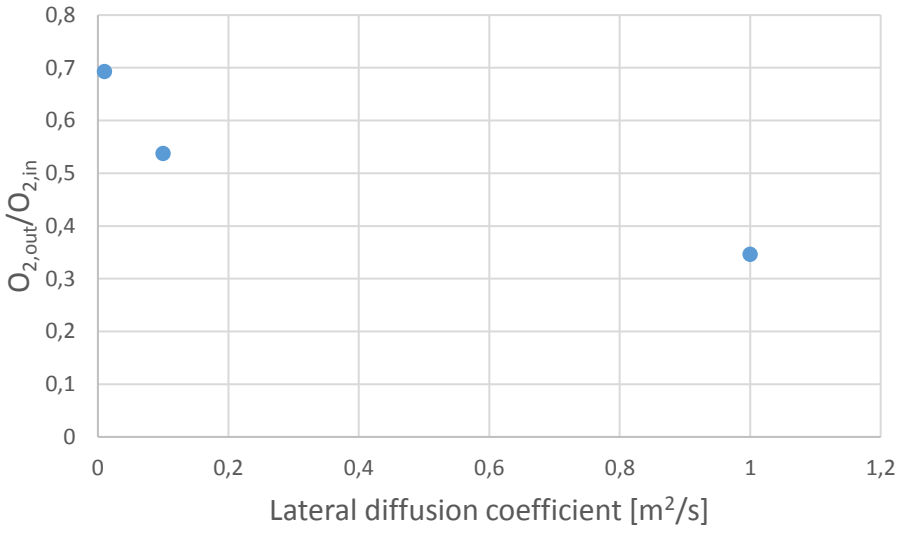

***Figure 29**: Normalized O_2 flow leaving the combustor as function of the gas lateral diffusion coefficient*

As expected from the previous results, the high diffusion coefficient value gives the lowest value of unburnt oxygen at the reactor's inlet, although the value is not as low as in Case 2, see Figure 20, which suggests that velocity is a more sensitive parameter for combustion quality than the diffusion coefficient. This is confirmed by comparing the flow out of H_2 and CO in Case 2 and 7. In fact, in the low velocity case the flow leaving the reactor for the two species is much lower than the same species for Case 7, as shown in Table 5, although both represent a better alternative to the reference case, since the unburnt are reduced of one and three orders of magnitudes respectively for H_2 and CO.

***Table 5**: Unburnt H_2 and CO leaving the reactor for Case 1 (u=3.5 m/s, D_{lat}=0.1 m2/s), Case 2 (u=1 m/s, D_{lat}=0.1 m2/s) and Case 7 (u=3.5 m/s, D_{lat}=1 m2/s)*

Case	$H_{2\ out}\ /H_{2\ in}$	$CO_{out}\ /CO_{in}$
1	78.1%	20.5%
2	26%	0.05%
7	20.8%	0.02%

6 Conclusions

A 3-dimensional model for the gas flow in fluidized beds has been developed and implemented. The model considers two-phased gas flow in the dense bed and single-phased flow in the freeboard.

Four parameters have been analysed in this study for a bubbling fluidized bed reactor with heterogeneous injection of volatile gases: inlet gas velocity, gas exchange coefficient between phases in the dense bed, dense bed height and gas lateral dispersion.

Model results (Figs. 17 to 19) show that gas velocity at the inlet is a sensitive parameter, and, in particular, when lowering the velocity the gas concentration fields become more homogenous, since the mixing is improved as the residence time is higher.

As for the influence of the interphase gas exchange coefficient and of a higher dense bed (sections 5.4 and 5.5, respectively), the results showed very little or no influence, not even when doubling these with respect to the reference case (Fig. 21 to 24).

As for the gas lateral dispersion factor, it influences the mixing notably. In particular, with very low values there is little interaction between the two areas of injection, and outside from a narrow area across the injection boundary, the two sides can be considered as separate systems, with the main issue of leaving a high percentage of unburnt in the volatiles injection system (Figs. 25 to 27). A higher diffusion factor, instead, facilitates the mixing from the first stages of the reactor, and minimizes the unburnt problem at the exit, in particular for hydrogen (Fig. 28).

Hence, it can be said that the sensitive parameters in this study are the gas inlet velocity, which improves combustion when set to low values, and the gas lateral diffusion coefficient, for which on the other hand is preferable to have higher values. More in general, the system is primarily controlled by the mixing processes, while kinetics is not so influential. In fact, both cited parameters play an important role in mixing, and it has been observed in particular that velocity is more helpful for what concerns the amount of unburnt at the reactor's outlet.

6.1 Future development

In order to provide a more detailed study on conventional FB combustors, it would be needed to carry out a similar study with operational mode changed to CFB, as well as to inject the volatiles from the fuel feedings. Finally, a major development step would consist in accounting for active bulk solids in order to have a better comprehension of the phenomenon in e.g. CLC plants

7 References

[1] Royal Swedish academy of agriculture and forestry, (2015): Forests and forestry in Sweden, pp. 5

[2] International Energy Agency (2015) Carbon capture and storage: the solution for deep emission reduction

[3] The global CCS institute (2015) The global status of CCS. Summary report

[4] Global CCS Institute, (2016): The Global Status of CCS: 2016, Summary Report, Australia

[5] Carbon capture and storage association. What is CCS? Capture. Accessed 04/03/2017. URL: http://www.ccsassociation.org/

[6] Global CCS institute. Effects of CO2 capture efficiency of plant performance. Accessed 20/04/2017. URL: http://www.globalccsinstitute.com/

[7] Lyngfelt, A., Leckner, B., Mattisson, T. (2001) A fluidized-bed combustion process with inherent CO2 separation; Application of chemical-looping combustion. Chemical Engineering Science, Vol. 56, pp. 3101-3113

[8] J. M. Valverde (2012) Ca-based synthetic materials with enhanced CO_2 capture efficiency. Journal of Material Chemistry A, Vol. 1, pp. 447-468

[9] A. Perejón, L. M. Romeo, Y. Lara, P. Lisbona, A. Martínez, J. M. Valverde (2016) The Calcium-Looping technology for CO_2 capture: On the important roles of energy integration and sorbent behavior. Applied Energy, Vol. 162, pp. 787-807

[10] Valmet. Energy. Multifuel solutions. Accessed 11/05/2017. URL: http://www.valmet.com/

[11] Mattisson, T., Lyngfelt, A. (2001) Capture of CO2 using chemical-looping combustion. Department of energy conversion, Chalmers University of Technology, Göteborg, Sweden, 2001

[12] OpenEI, Energy information and data. Chemical looping. Accessed 27/04/2017. URL: http://en.openei.org/

[13] Versteeg, H. K., Malalasekera, W. (2007) An introduction to computational fluid dynamic

[14] H. Pálsson (2016) Three dimensional finite volume methodfor a linear transport equation

[15] Q. Fang, T. Tsuchiya, T. Yamamoro (2002) Finite difference, finite element and finite volume method applied to two-point boundary value problems

[16] Pallarès, D., Johnsson, F. (2013) Modeling of fluidized bed combustion processes

[17] Universität Münster. Accessed 5/06/2017. URL: https://www.uni-muenster.de/imperia/md/content/physik_tp/lectures/ws2016-2017/num_methods_i/appendix.pdf

[18] Petersen, I., Werther, J. (2005) Experimental investigation and modelling of gasification of sewage sludge in the circulating fluidized bed, Chemical Engineering and Processing, Vol. 44, pp. 731

[19] Henrik Thunman (2016) Compendium of Combustion engineering

[20] Kunii, D., Levenspiel, O. (2013) Fluidization engineering, 2nd edition

[21] Orcutt, J., Davidson, J., & Pigford, R. (1962). Reaction time distributions in fluidized catalytic reactors. In Chemical Engineering Progress Symposium Series (Vol. 58, pp. 1-15)

[22] Masayuki, H., Akira, N. (1987) A generalized bubble diameter correlation for gas-solid fluidized bed. AIChE Journal, Vol. 33, pp. 1868

[23] Lundberg, L., Pallarès, D., Johansson, R., Thunman, H. (2014) A 1-dimensional model of indirect biomass gasification in a dual fluidized bed system

[24] Wen, C. Y., Yu, Y. K., (1966) A generalized method for predicting the minimum fluidization velocity. AIChE Journal, Vol. 12, 610-612

[25] Welty, James R.; Wicks, Charles E.; Wilson, Robert E.; Rorrer, Gregory (2001). Fundamentals of Momentum, Heat, and Mass Transfer. Wiley

[26] Ratnasamy, Chandra; Wagner, Jon P. (2009). "Water Gas Shift Catalysis". Catalysis Reviews. 51 (3): 325–440.

[27] N.J. Higham (2002) Accuracy and stability of numerical algorithms, 2nd edition

[28] D. Pallarés, F. Johnsson (2015) Time-resolved modeling of gas mixing in fluidized bed units. Fuel Processing Technology, Vol. 134, pp. 73-84

[29] K. Myöhänen, T. Hyppänen (2011) A three-dimensional model frame for modelling combustion and gasification in circulation fluidized bed furnaces. International Journal of Chemical Engineering, Vol. 9

[30] Hannes, J. (1996) Mathematical modelling of circulating fluidized bed combustion